


Inorganic Chemistry

pubs.acs.org/IC

Article


Near Isotropic D_{4d} Spin Qubits as Nodes of a Gd(III)-Based Metal–Organic Framework

Javier López-Cabrelles, Luis Escalera-Moreno, Ziqi Hu, Helena Prima-García, Guillermo Mínguez Espallargas,* Alejandro Gaita-Ariño,* and Eugenio Coronado

 Cite This: *Inorg. Chem.* 2021, 60, 8575–8580

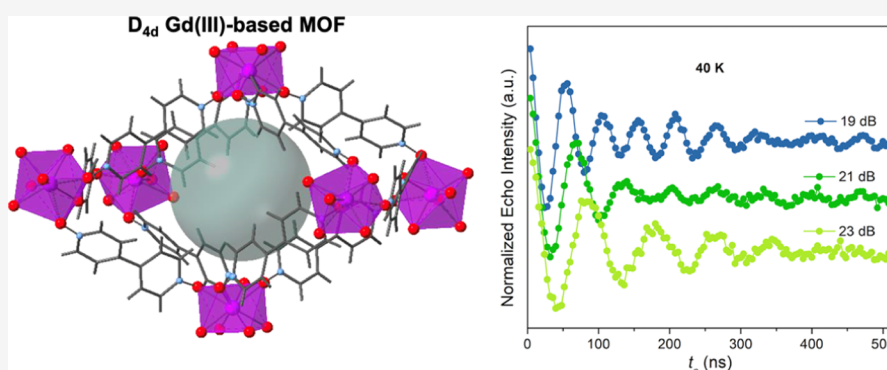
 Read Online

ACCESS |

 Metrics & More

 Article Recommendations

 Supporting Information



ABSTRACT: Embedding coherent spin motifs in reproducible molecular building blocks is a promising pathway for the realization of quantum technologies. Three-dimensional (3D) MOFs are a versatile platform for the rational design of extended structures employing coordination chemistry. Here, we report the synthesis and characterization of a gadolinium(III)-based MOF, $[\text{Gd}(\text{bipyNO})_4](\text{TfO})_3 \cdot x\text{MeOH}$ (bipyNO = bipyridine, N,N' -dioxide; TfO = triflate; and MeOH = methanol) (**quMOF-1**), which presents a unique coordination geometry that leads to a tiny magnetic anisotropy (in terms of D , an equivalent zero-field splitting would be achieved by $D = 0.006 \text{ cm}^{-1}$) even compared with regular Gd(III) complexes. Pulsed electron paramagnetic resonance experiments on its magnetically diluted samples confirm the preservation of quantum coherence of single Gd(III) qubit units in this 3D extended molecular architecture ($T_2 = 612 \text{ ns}$ and $T_1 = 66 \mu\text{s}$ at 3.5 K), which allows for the detection of Rabi oscillations at 40 K.

INTRODUCTION

Qubits, or quantum two-level systems, are the basic building block units of the next generation of quantum devices. However, in order to make them useful, it is necessary to achieve their organization in specific ways. In this respect, magnetic molecules and molecular-based compounds are exquisitely complex quantum materials with unmatched potential.^{1–3} Metal–organic frameworks (MOFs)⁴ are crystalline solids with ample chemical flexibility, which may be suitable for the three-dimensional (3D) organization of molecular spin qubits in a way that allows nontrivial interactions. As magnetic MOFs⁵ permit the controlled construction of scalable spin structures from molecular building blocks, qubits-on-MOFs (for short: quMOFs) offer improved capabilities from the point of view of quantum information compared to zero-dimensional systems. However, there are problems with this simplified view. If the individual qubits within the MOF are heavily diluted by employing Y^{3+} as a diamagnetic analogue, either to allow individual addressability or long enough coherence times, the system is not more

ordered than nitrogen-vacancy (NV) impurities in diamond. On the contrary, if the qubits have unity concentration, then it will be impossible to address them individually as would be required in conventional “quantum circuit” schemes. Less conventional schemes that work with connected qubits in 1, 2, or higher dimensions have been studied theoretically and found to have some advantages, which would eventually be the path for the use of quMOFs.⁶ Furthermore, it has been proposed that quMOFs could display unusual behaviors in terms of phonon decoherence, the dominant source of spin relaxation at high temperatures.⁷

The possibility of using quMOFs as a platform for molecular spin qubits was recognized in 2014, albeit since then, it has

Received: February 18, 2021

Published: June 7, 2021



scarcely been experimentally investigated. We first proposed this possibility in the family of MOFs with formula $[\text{Ln}(\text{bipyNO})_4](\text{TfO})_3 \cdot \text{solvent}$ ($\text{Ln} = \text{Tb}, \text{Dy}, \text{Ho}, \text{and Er}$; $\text{bipyNO} = \text{bipyridine}, N, N'$ -dioxide and $\text{TfO} = \text{triflate}$),⁸ which is formed by a regular arrangement of single-ion magnets (SIMs). At the same time, quantum tunneling of magnetization in a different SIM–MOF was independently reported, albeit with no mention of qubits.⁹ It is only recently that the potential of quMOFs has started to be experimentally tested.^{10–15} While in this context, MOFs can also be exploited as quantum sensors; their characterization in terms of spin dynamics reveals a promising potential for quantum information processing. For instance, in the reported quMOF $[(\text{T CPP})\text{Co}_{0.07}\text{Zn}_{0.93}]_3[\text{Zr}_6\text{O}_4(\text{OH})_4(\text{H}_2\text{O})_6]_2$ [$\text{T CPP} = 5,10,15,20$ -tetrakis(carboxyphenyl)porphyrin], the qubit can be defined in the form of an atomic clock transition between two given spin states.¹¹ This allows for reaching $T_1 = 34 \mu\text{s}$ and $T_2 = 14 \mu\text{s}$ values for the spin–lattice and spin–spin relaxation times even at high spin concentrations, an unprecedented finding in this kind of magnetic system.

Long relaxation times in atomic clock transitions are just one of the demonstrations that the chemical control over the coordination sphere can directly affect spin dynamics. Recent works have demonstrated how chemistry can be employed to engineer the electronic structure and minimize the orbital angular momentum of molecular spin qubits to their prolonged relaxation times.^{16,17} In these works, intrinsically spin-only (pure ^2S states) systems are employed, such as Zn^{2+} ions, encapsulated in a porous zeolite structure to obtain phase memory times of up to $2 \mu\text{s}$ at room temperature.¹⁷ Robust spin dynamics are linked to the intrinsically isotropic electronic structure due to quenching of the orbital angular momentum in the ground state. It is not straightforward how to go down this route for systems with $S > 1/2$, but natural tools would include choosing a system with a weak orbital moment, such as an f^7 lanthanide ion, and a coordination environment with maximum cancellation of the ligand field due to symmetry reasons. In previous works, we demonstrated how the weak magnetic anisotropy of the $S = 7/2$ Gd^{3+} ion can be tuned by molecular design.¹⁸

In this work, we present the structural, theoretical, and electron paramagnetic resonance (EPR) characterization of a quMOF, the Gd^{3+} member of the MOF $[\text{Ln}(\text{bipyNO})_4](\text{TfO})_3 \cdot \text{MeOH}$ (from now on, **quMOF-1**).

RESULTS AND DISCUSSION

quMOF-1 is a crystalline 3D structure that is prepared in quantitative yields upon slow diffusion of the solvent, following the reported procedure.¹⁹ In this structure, which crystallizes in the $P1$ space group, each bipyNO linker forms bridges between pairs of different lanthanoids, with Gd – Gd distances of about 13 \AA . The 3D complex network has very large cavities that represent over 70% of the total volume (Figure 1), which are filled with the triflate counterions and solvent molecules, but which are susceptible to substitution to explore spin–lattice relaxation phenomena.⁶ The presence of triflate anions permits an ion exchange replacing that species with polyoxometalates,¹⁹ in particular $[\text{W}_6\text{O}_{19}]^{2-}$. These bigger anions confer better robustness to the material, preventing the collapse of the crystal structure, as shown by X-ray powder diffraction (Figure S1).

Single crystal analysis reveals the presence of three crystallographically independent Gd ions (Gd1 , Gd2 , and

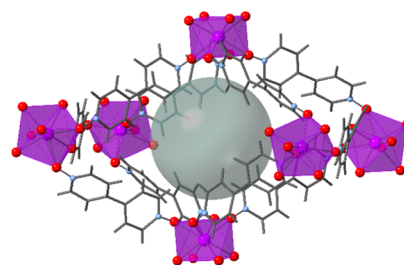


Figure 1. Crystal structure of **quMOF-1**. The Gd centers are shown as purple square antiprisms, the oxygen and nitrogen atoms as red and blue spheres, respectively, and carbon and hydrogen atoms as gray sticks. The light gray sphere represents the void space, which is filled with counterions and solvent molecules.

Gd3), each of which presents eightfold coordination by oxygen atoms belonging to the dioxide linker with very similar coordination spheres but presenting a different orientation in the space (Figure S3). The three coordination sites are extremely similar to each other, showing a structure unusually close to a semiregular anticube geometry, that is, a particular square antiprism that results from applying a 45° torsion to an ideal cube. This opposes compressed or elongated square antiprisms, more commonly found in coordination complexes. In other words, all coordinating atoms are practically at the so-called “magic angle” in spherical coordinates.

Most likely, this semiregular anticube coordination geometry is a consequence of using a unique monodentate ligand in the MOF structure²⁰ and has notable consequences for the expected crystal field Hamiltonian. First of all, the near- D_{4d} symmetry means that all extradiagonal terms of the crystal field Hamiltonian are expected to be close to zero. On its own, this would lead to limit the Hamiltonian to three nonvanishing zero-field splitting (ZFS) parameters: B_2^0 , B_4^0 , and B_6^0 . Additionally, positioning all donor atoms at the “magic angle” that is characteristic of the semiregular anticube geometry means that the second-order diagonal crystal field parameter, B_2^0 , is also expected to be negligible, resulting in a dramatically decreased anisotropy, even compared with regular Gd^{III} complexes, which are intrinsically weakly anisotropic due to their lack of angular momentum L .²¹

However, these two nonvanishing terms B_4^0 and B_6^0 , derived from coordination symmetry, cannot account for the collected X-band EPR data. A reasonable fit is achieved by introducing a fourth-order extradiagonal term B_4^4 . This is likely due to the slight deviation of the Gd^{3+} coordination sphere from a pure D_{4d} symmetry. An effective spin Hamiltonian is used to reproduce the shape of the spectrum: $H = B_4^4 O_4^4 + \mu_B g B \cdot S$, where O_4^4 is the extradiagonal extended Stevens operator of order 4 and range 4, and the second term is Zeeman splitting. The fit of the X-band continuous-wave (CW)-EPR spectrum as shown in Figure 2 results in an isotropic g factor of 1.983 and $B_4^4 = 11 \text{ MHz}$. This corresponds to a splitting of the ground and the first excited M_J doublets of 0.012 cm^{-1} . In terms of D , an equivalent ZFS would be achieved by $D = 6 \cdot 10^{-3} \text{ cm}^{-1}$. The extremely small ZFS effect of **quMOF-1** is distinct from those of most reported Gd^{3+} complexes^{18,21,22} but is comparable to that of $[\text{Gd}(\text{phendo})_4](\text{NO}_3)_3 \cdot n\text{MeOH}$, which also possesses a nearly perfect high symmetry (C_4) of the Gd^{3+} coordination sphere.²³ The g factor slightly smaller than 2.0 can also be observed in some of the abovementioned Gd^{3+} complexes.^{22,23}

After establishing the potential of **quMOF-1** as a qubit, the spin dynamics of the system has been studied with pulse EPR

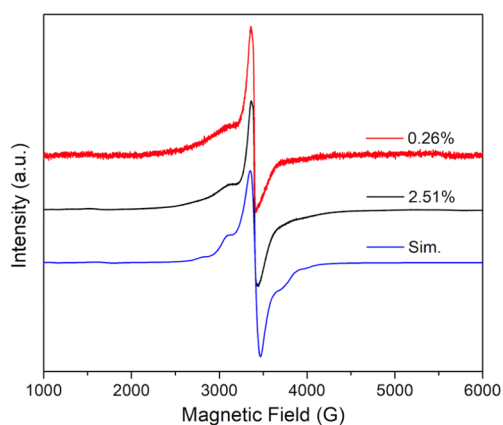


Figure 2. CW-EPR and simulated spectra of $[Y_{(1-x)}Gd_x(bipyNO)_4]-(TfO)_3 \cdot MeOH$ with $x = 2.51$ and 0.26% , recorded with a X-band EPR spectrometer (9.47 GHz) at 8 K.

in order to obtain the characteristic relaxation times T_1 and T_2 . These relaxation times are generally governed by two main decoherence sources affecting spin qubits, namely, the phonon bath and the spin bath. The spin bath is dominated by the interaction with neighboring nuclear and electron spins, which was studied by diluting **quMOF-1** in its yttrium diamagnetic analogue, $[Y_{(1-x)}Gd_x(bipyNO)_4](TfO)_3 \cdot MeOH$. Two different Gd concentrations have been used, namely, 2.51 and 0.26% (see Supporting Information for the synthetic experimental details). On the other hand, the effect of the phonon bath has been studied by measuring the spin dynamics at different temperatures.

To investigate the effects of concentration and temperature on T_1 and T_2 in these diluted compounds, inversion recovery and Hahn echo experiments were performed (Figures S6 and S10). T_1 and T_2 were fitted with a standard single-exponential model for all dilutions and temperatures. The extracted T_1 and T_2 values are reported in Figure 3. Strong temperature dependence of T_1 can be observed, spanning over one order of magnitude, with a significant maximum value of $T_1 = 65.8 \mu s$ at 3.5 K for $x = 0.26\%$, which drops to $2.9 \mu s$ as the temperature increases to 12 K. In contrast, T_2 has weaker temperature dependence, featuring an almost linear decrease upon warming

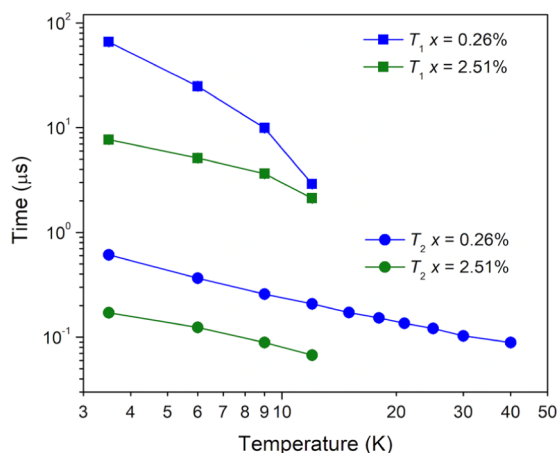


Figure 3. Experimental T_1 and T_2 values for diluted **quMOF-1** at two different gadolinium concentrations and temperatures. The error bars are within the size of symbols. Note the logarithmic scale of the X- and Y-axes.

when both time and temperature have logarithm scales. With a salient difference between the values of T_1 and T_2 in the 3.5–10 K temperature range, we can anticipate prior to any numerical analysis that T_2 is not limited by T_1 below 10 K, revealing a relaxation mechanism that exclusively influences T_2 . At higher temperatures, T_1 approaches T_2 , as is the case for a lot of different species other than V^{IV} and Cu^{II} complexes.²⁴ We further investigated the influence of instantaneous diffusion in T_2 by changing the π pulse length in the sequence applied. The result shown in Figure S8 indicates that this effect is negligible in low concentration ($x = 0.26\%$), while weakly active in the less diluted sample ($x = 2.51\%$). In addition, a close inspection of the Hahn echo measurements reveals the presence of electron spin echo envelope modulation, a behavior that arises when the electron spin couples with nearby hydrogen nuclei (Figure S9).²⁵

Finally, nutation experiments were also performed to verify whether the observed coherence times persist not only during the free precession of the spins but also in the presence of a driving field (Figure 4a). Indeed, any nontrivial quantum operation will involve a long series of spin rotations, which tend to result in faster echo decay, especially at high microwave powers. Remarkably, Rabi oscillations were clearly observed not only at a low temperature (Figure S11) but also at 40 K (Figure 4b). Their frequencies were derived from Fourier transforms (Figure 4c) to show linear dependence on B_1 . The detection of Rabi oscillations manifests that the coherent manipulation of the spin states in **quMOF-1** ($x = 0.26\%$) is feasible up to 40 K. However, it is impossible to individually address different transitions within this $S = 7/2$ system due to the tiny anisotropy, as illustrated in the single Rabi frequencies at 40 K (Figure 4c). This means that the conventional quantum circuit approach dealing with single-qubit operations would need to be dropped in favor of higher dimensionality schemes similar to the one indicated in the introduction.⁶

An attempt to theoretically rationalize the measured T_2 (T_2^{exp}) values was made by simulating the contribution to spin decoherence of the magnetic nuclei in the sample as well as of the Gd^{3+} electron spin bath; in the last case, in the form of instantaneous diffusion between pairs of dipole-coupled pairs of Gd^{3+} ions, both at $T \sim 3$ K.²⁶ This was performed using a customized version of SIMPRE1.2.²⁷ The calculated T_2 value considering only the nuclear spin bath ($T_2^{theo,n} \sim 350 \mu s$) reveals that the magnetic nuclei bath does not determine the experimentally observed quantum coherence because the T_2^{exp} values are 3 orders of magnitude smaller ($T_2^{exp} \sim 0.6 \mu s$). On the other hand, the calculated T_2 values considering the electronic spin bath ($T_2^{theo,e}$ in short) show a linear relationship with the Gd^{3+} concentration ($0 < x < 1$). Because instantaneous diffusion becomes more relevant as the metal ion concentration is increased, the $T_2^{theo,e}$ values get closer to the experimentally determined ones as x changes from 0.26 to 2.51% ($T_2^{exp} \sim 0.6$ and $0.1 \mu s$, respectively, see Figure 3). Indeed, we found $T_2^{theo,e} = 4.6$ and $0.48 \mu s$, respectively. As can be seen, at the highest Gd^{3+} ion concentration explored, the calculated $0.48 \mu s$ starts being in the same order of magnitude as the experimental value. Despite the disagreement of the values, this trend indicates that instantaneous diffusion is in competition with other mechanisms at limiting the qubit coherence because T_2^{exp} values are not fully recovered. Among the other decoherence sources, one should discard spin diffusion, namely, energy-conserving flip-flops between nuclear spin pairs but also involving the Gd^{3+} ions because no

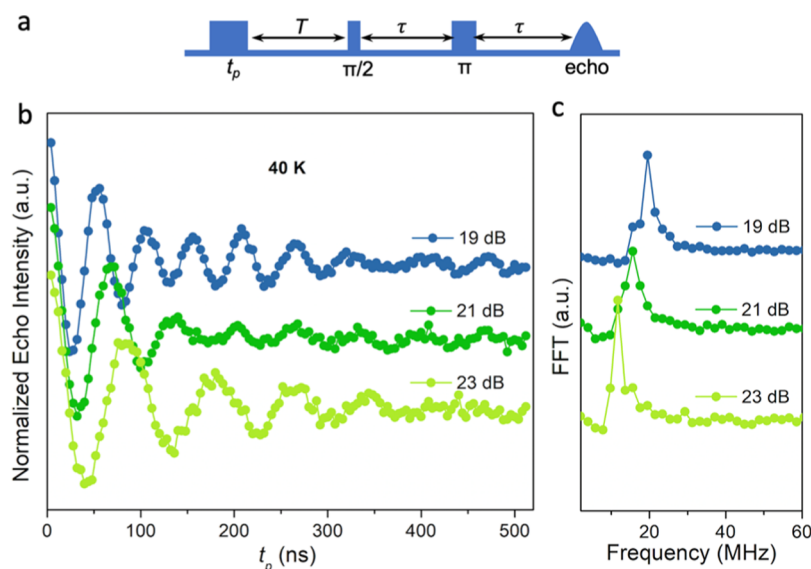


Figure 4. (a) Nutation pulse sequence used to observe Rabi oscillations in diluted **quMOF-1** ($x = 0.26\%$). (b) Nutation experiment measured at 40 K and a magnetic field of $B_0 = 3500$ G (main resonance line) using different microwave powers. (c) Corresponding Fourier transforms.

stretching factors greater than two were required to fit the intensity decays of the Hahn echo (Figure S6).²⁸ Instead, the competing contribution to decoherence could be present in the form of physical motions of magnetic nuclei that couple with spin qubits.^{29–31} Because T_1 is around 2 orders of magnitude above T_2^{exp} as shown in Figure 3, phonon-induced decoherence is not expected to be a crucial dephasing source in T_2^{exp} . Yet, it could be significant enough to produce the slight thermal dependence of T_2^{exp} .

CONCLUSIONS

In the present work, we have explored the quantum coherence properties of a Gd(III) MOF, namely, **quMOF-1**. This Gd(III)-based MOF is prepared using only bipyNO monodentate ligands, resulting in a nearly ideal semiregular anticube D_{4d} symmetry of the coordination sphere rarely seen in conventional complexes. This distinct feature makes it possible for the magnetic anisotropy of the Gd(III) MOF to be exceptionally weak, as characterized by X-band EPR spectroscopy. **quMOF-1** has a low spin density due to heavy polyoxometalate (POM) that is employed to stabilize it; this strategy may have future interest for applications in magneto cooling. Indeed, in adiabatic demagnetization, the lowest attainable temperature is limited first by the presence of magnetic interactions that bring about magnetic order below a critical temperature but also by magnetic anisotropy. If the goal is achieving a magnetic refrigerant material that can cool down devices in the order of milliKelvin, magnetic anisotropy ideally should be negligible because the smaller the anisotropy, the less pronounced are the crystal field effects which, splitting the energy levels, result in maxima of the magnetocaloric effect at lower temperatures.³² With the currently achieved anisotropy, in terms of D , being equally $D = 6 \times 10^{-3} \text{ cm}^{-1}$ ($D = 8.6 \times 10^{-3} \text{ K}$), this kind of coordination geometry would be ideal to cool down to temperatures around 10 mK.

Furthermore, this 3D organization of isotropic qubits, diluted in its diamagnetic yttrium analogue, exhibits quantum coherence ($T_2 = 612$ ns and $T_1 = 66$ μs at 3.5 K) and Rabi oscillations up to 40 K. Although this system is in a typical T_2 range (from hundreds of nanoseconds to microseconds) for

Gd³⁺ complexes,^{18,21–23,33} which are orders of magnitude below the record molecular spin qubit of the millisecond scale,^{34,35} this work is a step forward in the road toward scaling up spin qubits into extended molecular arrays. Our theoretical estimates suggest that besides instantaneous diffusion, its coherence time is likely limited by the physical motions of magnetic nuclei coupling with spin qubits, suggesting that the quantum coherence may be further improved by avoiding these motions.

EXPERIMENTAL SECTION

Synthesis. To prepare two ratios of Gd/Y, different solid solutions were prepared. A solid mixture of gadolinium triflate hydrate (0.005 mmol; 3 mg) and yttrium triflate hydrate (0.55 mmol; 297 mg) was first prepared (**Solid 1**). 6 mg of **Solid 1** was mixed with 54 mg of yttrium triflate (0.0001 mmol of Gd and 0.1 mmol of Y) (**Solid 2**). 30 mg of the solid solution {**Solid 1** for $[\text{Y}_{0.975}\text{Gd}_{0.025}(\text{bipyNO})_4]_3(\text{TfO})_9$ and **Solid 2** for $[\text{Y}_{0.9975}\text{Gd}_{0.0025}(\text{bipyNO})_4]_3(\text{TfO})_9$ } was carefully covered with dichloromethane (CH_2Cl_2 , 8 mL). Then, a layer of pure MeOH (8 mL) was stacked slowly, and on top of this, previously dissolved MeOH solution (17 mL) containing 4,4'-bipyridine- N,N' -dioxide (bipyNO, 0.18 mmol; 37.1 mg) was added. After three days, crystals suitable for single-crystal XRD were obtained.

Anion Exchange. Crystals of POM $(\text{TBA})_2[\text{W}_6\text{O}_{19}]$ were synthesized as previously reported.³⁶ The anion exchange processes were carried out by dissolving ca. 50 mg of this POM in acetonitrile (5 mL) yielding a clear solution in all cases. Then, single crystals of **quMOF-1-x** (1 mg) were added to each solution; and the color of the crystals began to change to clear brown.

EPR Measurements. X-band continuous-wave and pulsed EPR data were recorded on an ELEXSYS E580 EPR spectrometer (Bruker) equipped with a pulsed X-band (9.70 GHz cavity and resonators) operating in the range 4–300 K. The CW EPR powder spectra were simulated by EasySpin toolbox³⁷ (<http://www.easyspin.org/>) based on Matlab.

Field-swept electron spin echo-detected EPR spectra were recorded using a two-pulse echo sequence ($\pi/2 - \tau - \pi - \tau - \text{echo}$) with microwave pulse lengths of 16 ns and 32 ns and an interpulse time $\tau = 200$ ns. The echo decay curves were collected by application of the abovementioned sequence at the field of maximum echo intensity at variable temperatures with varying τ (starting from $\tau = 200$ ns). T_1 values were obtained at the main resonances using a three-pulse inversion recovery sequence ($\pi - T - \pi/2 - \tau - \pi - \tau - \text{echo}$) with $\tau = 500$

ns and with the four-step phase cycling. Rabi oscillations were performed using a variable-length nutation pulse (t_p) within the standard sequence ($t_p - T - \pi/2 - \tau - \pi - \tau$ -echo) at different attenuations of the microwave power. In all experiments, we applied an external magnetic field $B_0 = 3500$ G.

Continuous Shape Measure Calculations. The shape measures have been calculated with SHAPE (version 2.1).³⁸ The coordinates for oxygen and gadolinium have been extracted from the crystal structure data.¹⁹ Square antiprism is the shape with the minimum value.

Theoretical Calculations. The theoretical estimates of T_2 were performed by employing home-mode software package SIMPRE1.2 with a magnetic field magnitude of 0.35 T.²⁷ The nuclear spin bath is composed of the crystallographic positions of all the magnetic nuclei inside a sphere of a given radius. The radii selected by us were 30, 50, and 60 Å. The first value was enough to converge the calculated $T_2^{\text{theo},n}$ values, which means that further increasing the sphere radius does not produce any significant change in $T_2^{\text{theo},n}$ anymore, and hence, sample-shape dependencies are safely removed. The Gd^{3+} ion bath is composed of the crystallographic positions of all the Gd^{3+} ions inside a sphere of a given radius. Note that this explicitly considers solvent molecules inside the pores. In this case, a radius of 1000 Å was enough to converge the calculated $T_2^{\text{theo},e}$ values for the three Gd^{3+} concentrations. To simulate a given Gd^{3+} concentration x inside the selected sphere, we need to remove the proper number of Gd^{3+} ions. For that, we sweep all the Gd^{3+} ion positions, and at each one, a random number p between 0 and 1 is generated. If $0 < p < x$, we save the given crystallographic position. Otherwise, we drop it. For each given Gd^{3+} concentration, the calculations are adapted to produce average $T_2^{\text{theo},e}$ values because the samples are measured in the form of solutions instead of single crystals.

■ ASSOCIATED CONTENT

SI Supporting Information

The Supporting Information is available free of charge at <https://pubs.acs.org/doi/10.1021/acs.inorgchem.1c00504>.

Synthesis procedures, structural analysis, and detailed EPR characterization (PDF)

■ AUTHOR INFORMATION

Corresponding Authors

Guillermo Mínguez Espallargas – Instituto de Ciencia Molecular (ICMol), Universitat de València, 46980 Paterna, Spain; orcid.org/0000-0001-7855-1003; Email: guillermo.minguez@uv.es

Alejandro Gaita-Ariño – Instituto de Ciencia Molecular (ICMol), Universitat de València, 46980 Paterna, Spain; orcid.org/0000-0002-1600-8627; Email: alejandro.gaita@uv.es

Authors

Javier López-Cabrelles – Instituto de Ciencia Molecular (ICMol), Universitat de València, 46980 Paterna, Spain

Luis Escalera-Moreno – Instituto de Ciencia Molecular (ICMol), Universitat de València, 46980 Paterna, Spain

Ziqi Hu – Instituto de Ciencia Molecular (ICMol), Universitat de València, 46980 Paterna, Spain; orcid.org/0000-0003-1830-1584

Helena Prima-García – Instituto de Ciencia Molecular (ICMol), Universitat de València, 46980 Paterna, Spain; orcid.org/0000-0002-3390-5370

Eugenio Coronado – Instituto de Ciencia Molecular (ICMol), Universitat de València, 46980 Paterna, Spain; orcid.org/0000-0002-1848-8791

Complete contact information is available at:

<https://pubs.acs.org/10.1021/acs.inorgchem.1c00504>

Author Contributions

J.L.C., L.E.M., and Z.H. contributed equally to this work. The manuscript was written through contributions of all authors. All authors have given approval to the final version of the manuscript.

Notes

The authors declare no competing financial interest.

■ ACKNOWLEDGMENTS

We acknowledge funding by the EU [ERC Consolidator grants DECRESIM (647301) and S-CAGE (724681)], the SUMO QUANTERA Project and FATMOLS (862893), Spanish MICINN (projects MAT2017-89993-R and CTQ2017-89528-P cofinanced by FEDER and Excellence Unit María de Maeztu CEX2019-000919-M), and the Generalitat Valenciana (PROMETEO/2019/066 and PROMETEO/2017/066, PO FEDER Program IDIFEDER/2018/061, IDIFEDER/2020/063 and IDIFEDER/2020/060). G.M.E. and A.G.A. acknowledge funding by MICINN (Ramón y Cajal Program). J.L.C. acknowledges the Universitat de València for an “Atracció de Talent” grant. L.E.M. acknowledges the Generalitat Valenciana for a VALi+d predoctoral grant.

■ REFERENCES

- Gaita-Ariño, A.; Luis, F.; Hill, S.; Coronado, E. Molecular Spins for Quantum Computation. *Nat. Chem.* **2019**, *11*, 301–309.
- Fataftah, M. S.; Freedman, D. E. Progress towards Creating Optically Addressable Molecular Qubits. *Chem. Commun.* **2018**, *54*, 13773–13781.
- Coronado, E. Molecular magnetism: from chemical design to spin control in molecules, materials and devices. *Nat. Rev. Mater.* **2020**, *5*, 87–104.
- (a) Maurin, G.; Serre, C.; Cooper, A.; Férey, G. The New Age of MOFs and of Their Porous-Related Solids. *Chem. Soc. Rev.* **2017**, *46*, 3104–3107. (b) Zhou, H.-C. J.; Kitagawa, S. Metal–Organic Frameworks (MOFs). *Chem. Soc. Rev.* **2014**, *43*, 5415–5418.
- (a) Mínguez Espallargas, G.; Coronado, E. Magnetic Functionalities in MOFs: From the Framework to the Pore. *Chem. Soc. Rev.* **2018**, *47*, 533–557. (b) Thorarindottir, A. E.; Harris, T. D. Metal–Organic Framework Magnets. *Chem. Rev.* **2020**, *120*, 8716.
- Raussendorf, R.; Harrington, J. Fault-Tolerant Quantum Computation with High Threshold in Two Dimensions. *Phys. Rev. Lett.* **2007**, *98*, 190504.
- Gaita-Ariño, A.; Prima-García, H.; Cardona-Serra, S.; Escalera-Moreno, L.; Rosaleny, L. E.; Baldoví, J. J. Coherence and Organisation in Lanthanoid Complexes: From Single Ion Magnets to Spin Qubits. *Inorg. Chem. Front.* **2016**, *3*, 568–577.
- Baldoví, J. J.; Coronado, E.; Gaita-Ariño, A.; Gamer, C.; Giménez-Marqués, M.; Mínguez Espallargas, G. A SIM-MOF: Three-Dimensional Organisation of Single-Ion Magnets with Anion-Exchange Capabilities. *Chem.—Eur. J.* **2014**, *20*, 10695–10702.
- Tian, Y.; Wang, W.; Chai, Y.; Cong, J.; Shen, S.; Yan, L.; Wang, S.; Han, X.; Sun, Y. Quantum Tunneling of Magnetization in a Metal–Organic Framework. *Phys. Rev. Lett.* **2014**, *112*, 017202.
- Graham, M. J.; Zadrozny, J. M.; Fataftah, M. S.; Freedman, D. E. Forging Solid-State Qubit Design Principles in a Molecular Furnace. *Chem. Mater.* **2017**, *29*, 1885–1897.
- Zadrozny, J. M.; Gallagher, A. T.; Harris, T. D.; Freedman, D. E. A Porous Array of Clock Qubits. *J. Am. Chem. Soc.* **2017**, *139*, 7089–7094.
- Yamabayashi, T.; Atzori, M.; Tesi, L.; Cosquer, G.; Santanni, F.; Boulon, M.-E.; Morra, E.; Benci, S.; Torre, R.; Chiesa, M.; Sorace, L.; Sessoli, R.; Yamashita, M. Scaling Up Electronic Spin Qubits into a

Three-Dimensional Metal–Organic Framework. *J. Am. Chem. Soc.* **2018**, *140*, 12090–12101.

(13) Urtizberea, A.; Natividad, E.; Alonso, P. J.; Andrés, M. A.; Gascón, I.; Goldmann, M.; Roubeau, O. A Porphyrin Spin Qubit and Its 2D Framework Nanosheets. *Adv. Funct. Mater.* **2018**, *28*, 1801695.

(14) Urtizberea, A.; Natividad, E.; Alonso, P. J.; Pérez-Martínez, L.; Andrés, M. A.; Gascón, I.; Gimeno, I.; Luis, F.; Roubeau, O. Vanadyl Spin Qubit 2D Arrays and Their Integration on Superconducting Resonators. *Mater. Horiz.* **2020**, *7*, 885–897.

(15) Yu, C.-J.; Krzyaniak, M. D.; Fataftah, M. S.; Wasielewski, M. R.; Freedman, D. E. A Concentrated Array of Copper Porphyrin Candidate Qubits. *Chem. Sci.* **2019**, *10*, 1702–1708.

(16) Ariciu, A.-M.; Woen, D. H.; Huh, D. N.; Nodaraki, L. E.; Kostopoulos, A. K.; Goodwin, C. A. P.; Chilton, N. F.; McInnes, E. J. L.; Winpenny, R. E. P.; Evans, W. J.; Tuna, F. Engineering Electronic Structure to Prolong Relaxation Times in Molecular Qubits by Minimising Orbital Angular Momentum. *Nat. Commun.* **2019**, *10*, 3330.

(17) Morra, E.; Berlier, G.; Borfecchia, E.; Bordiga, S.; Beato, P.; Chiesa, M. Electronic and Geometrical Structure of Zn²⁺ Ions Stabilized in the Porous Structure of Zn-Loaded Zeolite H-ZSM-5: A Multifrequency CW and Pulse EPR Study. *J. Phys. Chem. C* **2017**, *121*, 14238–14245.

(18) Martínez-Pérez, M. J.; Cardona-Serra, S.; Schlegel, C.; Moro, F.; Alonso, P. J.; Prima-García, H.; Clemente-Juan, J. M.; Evangelisti, M.; Gaita-Ariño, A.; Sesé, J.; van Slageren, J.; Coronado, E.; Luis, F. Gd-Based Single-Ion Magnets with Tunable Magnetic Anisotropy: Molecular Design of Spin Qubits. *Phys. Rev. Lett.* **2012**, *108*, 247213.

(19) López-Cabrelles, J.; Mínguez Espallargas, G.; Coronado, E. Single-Crystal-to-Single-Crystal Anion Exchange in a Gadolinium MOF: Incorporation of POMs and [AuCl₄][−]. *Polymers* **2016**, *8*, 171.

(20) When eight charges are distributed on the surface of a (coordination) sphere in a way that maximises the distance between them, i.e. maximizing the metal–ligand interaction and minimising the ligand–ligand repulsion, the resulting polyhedron corresponds to a semiregular anticube, which is the particular case of square anti-prism where all interatomic distances are equal.

(21) Jenkins, M. D.; Duan, Y.; Diosdado, B.; García-Ripoll, J. J.; Gaita-Ariño, A.; Giménez-Saiz, C.; Alonso, P. J.; Coronado, E.; Luis, F. Coherent Manipulation of Three-Qubit States in a Molecular Single-Ion Magnet. *Phys. Rev. B* **2017**, *95*, 064423.

(22) Hu, Z.; Dong, B.-W.; Liu, Z.; Liu, J.-J.; Su, J.; Yu, C.; Xiong, J.; Shi, D.-E.; Wang, Y.; Wang, B.-W.; Ardavan, A.; Shi, Z.; Jiang, S.-D.; Gao, S. Endohedral Metallofullerene as Molecular High Spin Qubit: Diverse Rabi Cycles in Gd₂@C₇₉N. *J. Am. Chem. Soc.* **2018**, *140*, 1123–1130.

(23) Handzlik, G.; Magott, M.; Arczyński, M.; Sheveleva, A. M.; Tuna, F.; Sarewicz, M.; Osyczka, A.; Rams, M.; Vieru, V.; Chibotaru, L. F.; Pinkowicz, D. Magnetization Dynamics and Coherent Spin Manipulation of a Propeller Gd(III) Complex with the Smallest Helicene Ligand. *J. Phys. Chem. Lett.* **2020**, *11*, 1508–1515.

(24) (a) Shiddiq, M.; Komijani, D.; Duan, Y.; Gaita-Ariño, A.; Coronado, E.; Hill, S. Enhancing Coherence in Molecular Spin Qubits via Atomic Clock Transitions. *Nature* **2016**, *531*, 348–351.

(b) Zadrozny, J. M.; Freedman, D. E. Qubit Control Limited by Spin–Lattice Relaxation in a Nuclear Spin-Free Iron(III) Complex. *Inorg. Chem.* **2015**, *54*, 12027–12031.

(25) Schweiger, A.; Jeschke, G. *Principles of Pulse Electron Paramagnetic Resonance*; Oxford University Press, 2001

(26) (a) Stamp, P. C. E.; Tupitsyn, I. S. Coherence Window in the Dynamics of Quantum Nanomagnets. *Phys. Rev. B: Condens. Matter Mater. Phys.* **2004**, *69*, 014401. (b) Escalera-Moreno, L.; Gaita-Ariño, A.; Coronado, E. Decoherence from Dipolar Interspin Interactions in Molecular Spin Qubits. *Phys. Rev. B* **2019**, *100*, 064405.

(27) Cardona-Serra, S.; Escalera-Moreno, L.; Baldoví, J. J.; Gaita-Ariño, A.; Clemente-Juan, J. M.; Coronado, E. SIMPRE1.2: Considering the Hyperfine and Quadrupolar Couplings and the Nuclear Spin Bath Decoherence. *J. Comput. Chem.* **2016**, *37*, 1238–1244.

(28) Lenz, S.; Bader, K.; Bamberger, H.; van Slageren, J. Quantitative Prediction of Nuclear-Spin-Diffusion-Limited Coherence Times of Molecular Quantum Bits Based on Copper(II). *Chem. Commun.* **2017**, *53*, 4477–4480.

(29) Lin, C.-Y.; Ngendahimana, T.; Eaton, G. R.; Eaton, S. S.; Zadrozny, J. M. Counterion Influence on Dynamic Spin Properties in a V(IV) Complex. *Chem. Sci.* **2019**, *10*, 548–555.

(30) Zecevic, A.; Eaton, G. R.; Eaton, S. S.; Lindgren, M. Dephasing of Electron Spin Echoes for Nitroxyl Radicals in Glassy Solvents by Non-Methyl and Methyl Protons. *Mol. Phys.* **1998**, *95*, 1255–1263.

(31) Eaton, G. R.; Eaton, S. S. Solvent and Temperature Dependence of Spin Echo Dephasing for Chromium(V) and Vanadyl Complexes in Glassy Solution. *J. Magn. Reson.* **1999**, *136*, 63–68.

(32) Martínez-Pérez, M.-J.; Montero, O.; Evangelisti, M.; Luis, F.; Sesé, J.; Cardona-Serra, S.; Coronado, E. Fragmenting Gadolinium: Mononuclear Polyoxometalate-Based Magnetic Coolers for Ultra-Low Temperatures. *Adv. Mater.* **2012**, *24*, 4301–4305.

(33) Layfield, R. A.; Murugesu, M. *Lanthanides and Actinides in Molecular Magnetism*; John Wiley & Sons, 2015.

(34) Zadrozny, J. M.; Niklas, J.; Poluektov, O. G.; Freedman, D. E. Millisecond Coherence Time in a Tunable Molecular Electronic Spin Qubit. *ACS Cent. Sci.* **2015**, *1*, 488–492.

(35) Dai, Y.; Fu, Y.; Shi, Z.; Qin, X.; Mu, S.; Wu, Y.; Su, J.-H.; Deng, Y.-F.; Qin, L.; Zhai, Y.-Q.; Zheng, Y.-Z.; Rong, X.; Du, J. Experimental Protection of the Spin Coherence of a Molecular Qubit Exceeding a Millisecond. *Chin. Phys. Lett.* **2021**, *38*, 030303.

(36) *Inorganic Syntheses*; Ginsberg, A. P., Ed.; John Wiley & Sons, Inc.: Hoboken, NJ, USA, 1990; Volume 27

(37) Stoll, S.; Schweiger, A. EasySpin, a Comprehensive Software Package for Spectral Simulation and Analysis in EPR. *J. Magn. Reson.* **2006**, *178*, 42–55.

(38) Llundell, M.; Casanova, D.; Cirera, J.; Boffill, J. M.; Alemany, P.; Alvarez, S.; Pinsky, M.; Avnir, D. *SHAPE (2.1)*; Universitat de Barcelona: Spain, 2003.